

Dynamical properties of max-plus equations obtained from tropically discretized Sel'kov model

Shousuke Ohmori^{*)} and Yoshihiro Yamazaki

Department of Physics, Waseda University, Shinjuku, Tokyo 169-8555, Japan

**corresponding author: 42261timemachine@ruri.waseda.jp*

Abstract

Max-plus equations are derived from tropically discretized Sel'kov model via ultradiscretization. These max-plus equations possess common dynamical structures with the discretized model: Neimark-Sacker bifurcation and limit cycles. The limit cycles of the ultradiscrete max-plus equations have seven discrete states. Furthermore, these max-plus equations exhibit excitability. Relationship between the tropically discretized model and the derived max-plus equations is also discussed based on numerical results. It is found that the derived max-plus equations correspond to a limiting case of the tropically discretized model.

Ultradiscretization is known to be a method to derive max-plus equations from difference equations. Actually for example, ultradiscretization has been applied to a discretized KdV equation. As a result, a max-plus equation has been obtained, which is often referred as the box-and-ball system [1, 2]. The box-and-ball system (ultradiscrete system) exhibits soliton behaviors which are also confirmed in the original KdV equation (continuous system). The important point is that ultradiscretization successfully retains and elucidates the essence of dynamical structures in the original nonlinear systems (soliton behaviors in this example), although the ultradiscrete system does not reproduce all dynamical properties of the original system.

Non-integrable dissipative systems and reaction-diffusion systems have also been target for application of ultradiscretization [3, 4, 5, 6, 7, 8, 9, 10]. Recently, we have applied ultradiscretization to bifurcation phenomena in one-dimensional dynamical systems[10]. Bifurcation phenomena have been hugely studied from viewpoint of continuous[11, 12, 13] and discrete[14, 15, 16] dynamical systems. In our previous study, focusing on tropically discretized one-dimensional normal forms of saddle-node, transcritical, and pitchfork bifurcations, their ultradiscrete max-plus equations were derived and their dynamical properties were investigated. In particular, it is found that they possess “ultradiscrete bifurcations”, which are piecewise linear bifurcations for saddle-node, transcritical, and pitchfork types, respectively. These ultradiscrete bifurcations can be visually understood by piecewise linear graphs for the ultradiscrete max-plus equations.

In this letter, we focus on Neimark-Sacker bifurcation (N-S bifurcation hereafter) in two-dimensional dynamical systems by considering tropically discretized Sel’kov model as an example. (N-S bifurcation is often referred as Hopf bifurcation for maps or discrete dynamical systems.) From this discretized model, max-plus equations are derived by ultradiscretization. We show that the obtained max-plus equations exhibit N-S bifurcation, excitability, and existence of limit cycles. Furthermore, relationship between the discretized model and the derived max-plus equations is numerically discussed.

Let us start with introducing the tropically discretized Sel’kov model for (x_n, y_n) :

$$x_{n+1} = \frac{x_n + \tau(ay_n + x_n^2 y_n)}{1 + \tau}, \quad (1)$$

$$y_{n+1} = \frac{y_n + \tau b}{1 + \tau(a + x_n^2)}, \quad (2)$$

where a , b and τ are positive parameters. The positive integer n shows the iteration steps. It is confirmed that in the limit of $\tau \rightarrow 0$ these equations correspond to the continuous Sel’kov model

[12, 17]:

$$\frac{dx}{dt} = -x + ay + x^2y, \quad (3)$$

$$\frac{dy}{dt} = b - ay - x^2y, \quad (4)$$

where $x_n = x(n\tau) \rightarrow x(t)$ and $y_n = y(n\tau) \rightarrow y(t)$ for $\tau \rightarrow 0$. In eqs.(3) and (4), Hopf bifurcation occurs when a and b satisfy $b^2 = \frac{1}{2}(1 - 2a \pm \sqrt{1 - 8a})$ ($\equiv b_{\pm}^2(a)$), and limit cycle solutions are obtained for $b_-(a) < b < b_+(a)$.

In general, the tropical discretization can avoid appearance of negative values in the equations; otherwise the negative values make ultradiscretization impossible [4]. Ultradiscretization for eqs.(1)-(2) is performed in the following way. The variable transformations,

$$\tau = e^T, \quad x_n = e^{X'_n}, \quad y_n = e^{Y'_n}, \quad a = e^A, \quad b = e^{B'}, \quad (5)$$

are applied to eqs.(1)-(2), and the ultradiscretization

$$\ln(e^\alpha + e^\beta + \dots) \rightarrow \max(\alpha, \beta, \dots) \quad (6)$$

is carried out [18]. Then, we obtain

$$X'_{n+1} = \max(X'_n, T + \max(A + Y'_n, 2X'_n + Y'_n)) - \max(0, T), \quad (7)$$

$$Y'_{n+1} = \max(Y'_n, T + B') - \max(0, T + \max(A, 2X'_n)). \quad (8)$$

Additionally assuming as the condition of T that

$$T \geq \max\{0, -A, Y'_n - B', -(X'_n + Y'_n)\} \quad (9)$$

for all n , eqs. (7)-(8) become

$$X'_{n+1} = Y'_n + \max(A, 2X'_n), \quad (10)$$

$$Y'_{n+1} = B' - \max(A, 2X'_n). \quad (11)$$

After the variable transformations

$$X'_n - \frac{A}{2} = X_n, \quad Y'_n + \frac{A}{2} = Y_n, \quad \text{and} \quad B' - \frac{A}{2} = B, \quad (12)$$

we finally obtain the ultradiscrete max-plus equations for the tropically discretized Sel'kov model:

$$X_{n+1} = Y_n + \max(0, 2X_n), \quad (13)$$

$$Y_{n+1} = B - \max(0, 2X_n). \quad (14)$$

Now we discuss dynamical properties of eqs.(13)-(14). These equations are considered as a discrete dynamical system $\mathbf{x}_{n+1} = \mathbf{F}(\mathbf{x}_n)$ for the state variable $\mathbf{x}_n = (X_n, Y_n)$ by equipping the evolution operator $\mathbf{F} : (x, y) \mapsto (y + \max(0, 2x), B - \max(0, 2x))$. A trajectory $\{\mathbf{x}_0, \mathbf{x}_1, \mathbf{x}_2, \dots\} (\equiv \{\mathbf{x}_n\})$ from the initial point $\mathbf{x}_0 = (X_0, Y_0)$ is given by $\mathbf{x}_n = \mathbf{F}^n(\mathbf{x}_0) (n = 1, 2, \dots)$. Here (X_n, Y_n) plane is divided into the following two regions I: $X_n > 0$ and II: $X_n \leq 0$. In each region, eqs.(13)-(14) can be represented as the following matrix form.

(Region I) When $X_n > 0$, eqs. (13)-(14) can be rewritten as

$$\begin{pmatrix} X_{n+1} \\ Y_{n+1} \end{pmatrix} = \begin{pmatrix} 2 & 1 \\ -2 & 0 \end{pmatrix} \begin{pmatrix} X_n \\ Y_n \end{pmatrix} + \begin{pmatrix} 0 \\ B \end{pmatrix}, \quad (15)$$

where eq. (15) has the fixed point $\bar{\mathbf{x}}_I = (B, -B)$. The matrix $\mathbf{A}_I = \begin{pmatrix} 2 & 1 \\ -2 & 0 \end{pmatrix}$ satisfies $\text{Tr}\mathbf{A}_I = \det\mathbf{A}_I = 2$, where Tr and \det stand for trace and determinant of a matrix, respectively. Therefore, the trajectory given by eq.(15) is characterized as a clockwise spiral source[16], whose center is the unstable fixed point $\bar{\mathbf{x}}_I$; Fig. 1(a) shows a typical trajectory of $\{\mathbf{x}_n\}$.

(Region II) When $X_n \leq 0$, the matrix form of eqs. (13)-(14) is

$$\begin{pmatrix} X_{n+1} \\ Y_{n+1} \end{pmatrix} = \begin{pmatrix} 0 & 1 \\ 0 & 0 \end{pmatrix} \begin{pmatrix} X_n \\ Y_n \end{pmatrix} + \begin{pmatrix} 0 \\ B \end{pmatrix}. \quad (16)$$

Equation (16) has the fixed point $\bar{\mathbf{x}}_{II} = (B, B)$. For the matrix $\mathbf{A}_{II} = \begin{pmatrix} 0 & 1 \\ 0 & 0 \end{pmatrix}$, $\text{Tr}\mathbf{A}_{II} =$

$\det \mathbf{A}_{II} = 0$. The fixed point $\bar{\mathbf{x}}_{II}$ becomes a stable node. Actually for any $\mathbf{x}_0 = (X_0, Y_0)$,

it is readily found that $\mathbf{x}_1 = (Y_0, B)$ and $\mathbf{x}_2 = (B, B) = \bar{\mathbf{x}}_{II}$ as shown in Fig. 1 (b).

Taking these dynamical properties in regions I and II into account, bifurcation of eqs. (13)-(14) can be grasped as follows. (i) When $B \leq 0$, both $\bar{\mathbf{x}}_I$ and $\bar{\mathbf{x}}_{II}$ are in region II; $\bar{\mathbf{x}}_{II}$ becomes a fixed point, but $\bar{\mathbf{x}}_I$ does not. Then, eqs.(13)-(14) have a unique fixed point $\bar{\mathbf{x}}_{II} = (B, B)$. (i-a) When $\mathbf{x}_0 = (X_0, Y_0)$ belongs to “region II-1”, which means $X_0 \leq 0$ and $Y_0 \leq 0$, $\mathbf{x}_1 = (Y_0, B)$ and $\mathbf{x}_2 = (B, B) = \bar{\mathbf{x}}_{II}$. Then any initial point in region II-1 reaches $\bar{\mathbf{x}}_{II}$ with two iteration steps. (i-b) \mathbf{x}_0 in region I moves into region II-1 within four iteration steps as shown in Fig.2. Then, any initial point in region II-1 reaches $\bar{\mathbf{x}}_{II}$ within six steps. (i-c) When \mathbf{x}_0 is in “region II-2”, $X_0 \leq 0$ and $Y_0 > 0$, $\mathbf{x}_1 = (Y_0, B)$ belongs to region I. Therefore, \mathbf{x}_0 reaches $\bar{\mathbf{x}}_{II}$ within seven steps from the property (i-b). From (i-a)-(i-c), the fixed point $\bar{\mathbf{x}}_{II} = (B, B)$ is stable. The trajectories of $\{\mathbf{x}_n\}$ in this case are shown in Fig. 3. Figure 3 also shows that excitability appears when \mathbf{x}_0 is in region II-2. Figure 4 shows time evolutions of (X_n, Y_n) from two different initial conditions. It is found that excitability occurs in Fig.4(b) by comparing with Fig.4(a). (ii) When $B > 0$, $\bar{\mathbf{x}}_I = (B, -B)$ becomes a unique unstable fixed point. We find that there exist two clockwise periodic solutions, \mathcal{C} and \mathcal{C}_s as shown in Fig.5(a), which are composed of the following seven points, respectively: $\mathcal{C} = \{(B, B) \rightarrow (3B, -B) \rightarrow (5B, -5B) \rightarrow (5B, -9B) \rightarrow (B, -9B) \rightarrow (-7B, -B) \rightarrow (-B, B) [\rightarrow (B, B)]\}$, $\mathcal{C}_s = \{(\frac{B}{15}, B) \rightarrow (\frac{17B}{15}, \frac{13B}{15}) \rightarrow (\frac{47B}{15}, -\frac{19B}{15}) \rightarrow (5B, -\frac{79B}{15}) \rightarrow (\frac{71B}{15}, -9B) \rightarrow (\frac{7B}{15}, -\frac{127B}{15}) \rightarrow (-\frac{113B}{15}, \frac{B}{15}) [\rightarrow (\frac{B}{15}, B)]\}$. It is also found that a trajectory with any initial condition except for $\bar{\mathbf{x}}_I$ is finally absorbed in \mathcal{C} or \mathcal{C}_s . Therefore, \mathcal{C} and \mathcal{C}_s are limit cycles. Figure 5(b) shows trajectories from four different initial conditions; they finally converge into \mathcal{C} .

Regarding basins of \mathcal{C} and \mathcal{C}_s , we focus on the fact that any trajectory has a point with $Y_n = B$ at a certain iteration step n . In other words, a point on the line l_B , $\mathbf{x}_n = (X_n, B)$

exists in all trajectories. It is possible to prove that all trajectories with a point on l_B except for $(\frac{B}{15}, B)$ and $(\frac{17B}{15}, B)$ are finally absorbed into \mathcal{C} . And any trajectory with $(\frac{B}{15}, B)$ or $(\frac{17B}{15}, B)$ finally goes into \mathcal{C}_s . Therefore, there exist only two limit cycles \mathcal{C} and \mathcal{C}_s in eqs.(13)-(14).

Now we focus on the linear stability for the tropically discretized Sel'kov model. Equations (1) and (2) are considered as a discrete dynamical system with the three positive parameters a , b and τ . The fixed point (\bar{x}, \bar{y}) for the model is $\bar{x} = b, \bar{y} = \frac{b}{b^2 + a}$, and the Jacobian matrix at (\bar{x}, \bar{y}) is

$$\begin{pmatrix} \frac{2\tau\bar{x}\bar{y} + 1}{\tau + 1} & \frac{\tau(\bar{x}^2 + a)}{\tau + 1} \\ -\frac{2\tau\bar{x}(\bar{y} + b\tau)}{(\tau(\bar{x}^2 + a) + 1)^2} & \frac{1}{\tau(\bar{x}^2 + a) + 1} \end{pmatrix}. \quad (17)$$

N-S bifurcation occurs under the condition that the eigenvalues of this Jacobian matrix are complex and their absolute values are equal to 1. This condition can be expressed by a surface as a function of a , b and τ ; Fig.6 shows the numerical results. From this figure, the following features are confirmed. (i) N-S bifurcation occurs for arbitrary τ , even for $\tau \rightarrow +\infty$. (ii) When $\tau \rightarrow 0$, N-S bifurcation curve is exactly consistent with Hopf bifurcation curve of the continuous Sel'kov model, $b = b_{\pm}(a)$. (iii) When $\tau \rightarrow +\infty$, N-S bifurcation curve becomes $b = \sqrt{a}$, and a limit cycle emerges when $b > \sqrt{a}$.

For the limit cycles, relationship between eqs.(13)-(14) and eqs.(1)-(2) is numerically investigated. Here we show the case of $a = 0.01$ and $b = 0.98$ for example. These values of a and b bring about limit cycle solutions in the continuous limit ($\tau \rightarrow 0$) of eqs.(1)-(2), namely eqs.(3)-(4). It is found that limit cycles exist for arbitrary value of τ , although the number of states in the cycles varies depending on τ ; Fig. 7 shows four limit cycles with different values of τ . The state (x_n, y_n) in the limit cycle is expressed by introducing the phase $\theta_n(\tau)$ as

$$\theta_n(\tau) = \arctan \frac{\ln y_n - \ln \bar{y}}{\ln x_n - \ln \bar{x}}. \quad (18)$$

$\theta_n(\tau)$ takes a value in the range of $[0, 2\pi]$. Figure 8(a) shows the density of $\{\theta_n(\tau)\}$ in the

limit cycles as a function of τ . In this figure, the phase Θ_n of the seven states (X_n, Y_n) in the limit cycle \mathcal{C} of the max-plus equations eqs.(13)-(14) are also depicted with the red broken line segments, where Θ_n is defined as

$$\Theta_n = \arctan \frac{Y_n + B}{X_n - B}, \quad (19)$$

and now we set $B = 1$. Figure 8(a) shows that $\theta_n(\tau)$ seems to be in agreement with the case in the continuous limit (eqs.(3)-(4)) when $\tau \lesssim 10^{-1}$. On the other hand, ultradiscrete feature emerges when $\tau \gtrsim 10^3$ and $\theta_n(\tau) \approx \Theta_n$ for $\tau \gtrsim 10^4$. Actually, considering the following transformations

$$X_n^* = \frac{\ln x_n - \frac{\ln a}{2}}{\ln b - \frac{\ln a}{2}}, \quad Y_n^* = \frac{\ln y_n + \frac{\ln a}{2}}{\ln b - \frac{\ln a}{2}}, \quad (20)$$

(X_n^*, Y_n^*) is almost consistent with (X_n, Y_n) in \mathcal{C} as shown in Fig.8(b), where the two cases, $\tau = 10^6$ and $\tau \rightarrow +\infty$, are plotted. From Fig.8, it is concluded that the ultradiscrete max-plus equations (eqs.(13)-(14)) can be considered as the limiting equations of eqs.(1)-(2) for $\tau \rightarrow +\infty$. Note that the limit $\tau \rightarrow +\infty$ automatically satisfies the condition of T , eq.(9). The important point is that the dynamical structures of N-S bifurcation and the limit cycles retain for large τ , even for $\tau \rightarrow +\infty$.

In the limit of $\tau \rightarrow +\infty$, eqs.(1)-(2) become

$$x_{n+1} = (a + x_n^2) y_n, \quad (21)$$

$$y_{n+1} = \frac{b}{a + x_n^2}. \quad (22)$$

After the above variable transformations (eqs.(5)and(12)) for them, we obtain

$$X_{n+1} = Y_n + \ln(1 + e^{2X_n}), \quad (23)$$

$$Y_{n+1} = B - \ln(1 + e^{2X_n}). \quad (24)$$

Applying the above ultradiscretization, eq.(6), to eqs.(23)-(24), $\ln(1 + e^{2X}) \rightarrow \max(0, 2X)$, we

reproduce eqs.(13)-(14). In other words, validity of eqs.(13)-(14), or applicability of ultradiscretization, is judged whether the approximation $\ln(1 + e^{2X}) \approx \max(0, 2X)$ holds or not.

In summary, we have investigated dynamical properties of the max-plus equations derived from the tropically discretized Sel'kov model. The max-plus equations exhibit N-S bifurcation and possess limit cycles. These dynamical features are in common with the original discretized model. For dynamical properties of the max-plus equations for N-S bifurcation and emergence of limit cycles, the present results are just for the specific model. Further investigation will be necessary for generality of the present results. We note that the derived max-plus equations can be considered as the limiting equations of the discrete model for $\tau \rightarrow +\infty$. It is interesting that the tropical discretization gives us a framework for considering both the continuous limit ($\tau \rightarrow 0$) and the ultradiscrete limit ($\tau \rightarrow +\infty$). Especially Figs.6 and 8(a) suggest the possibility of discussing transition between continuous and ultradiscrete descriptions preserving some essential dynamical structures.

Acknowledgement

The authors are grateful to Prof. M. Murata, at Tokyo University of Agriculture and Technology, Prof. K. Matsuya at Musashino University, Prof. D. Takahashi, Prof. T. Yamamoto, and Prof. Emeritus A. Kitada at Waseda University for useful comments and encouragements. This work was supported by Sumitomo Foundation, Grant Number 200146.

References

- [1] T. Tokihiro, D. Takahashi, J. Matsukidaira, and J. Satsuma, Phys. Rev. Lett. **76** 3247 (1996).
- [2] S. Tsujimoto and R. Hirota, JPSJ **67** 1809 (1998).
- [3] T. Nagatani, Phys. Rev. E **58** 700 (1998).

- [4] M. Murata, J. Differ. Equations Appl. **19** 1008 (2013).
- [5] S. Ohmori and Y. Yamazaki, Prog. Theor. Exp. Phys. 08A01 (2014).
- [6] K. Matsuya and M. Murata, Discrete Contin. Dyn. Syst. B **20** 173 (2015).
- [7] M. Murata, J. Phys. A Math, Theor. **48** 255202 (2015).
- [8] S. Gibo and H. Ito, J. Theor. Biol. **378** 89 (2015).
- [9] S. Ohmori and Y. Yamazaki, J. Phys. Soc. Jpn. **85** 045001 (2016).
- [10] S. Ohmori and Y. Yamazaki, J. Math. Phys. **61** 122702 (2020)
- [11] J. Guckenheimer and P. Holmes, *Nonlinear Oscillations, Dynamical Systems, and Bifurcations of Vector Fields* (Springer, New York, 1983).
- [12] Steven. H. Strogatz, *Nonlinear Dynamics and Chaos* (Westview Press, U.S. 1994).
- [13] G. Nicolis, *Introduction to Nonlinear Science* (Cambridge Univ. Press 1995).
- [14] C. Robinson, *Dynamical systems -Stability, Symbolic Dynamics, and Chaos-, 2ed edition* (CRC Press, Florida 1999).
- [15] Yuri A. Kuznetsov, *Elements of Applied Bifurcation Theory* (Springer-Verlag, New York, 2010).
- [16] O. Galor, *Discrete Dynamical Systems* (Springer, New York 2010).
- [17] E. E. Sel'kov, Eur. J. Biochem. **4** 79 (1968).
- [18] Ultradiscretization, eq.(6), can be formally described as shown in [1]

$$\lim_{\varepsilon \rightarrow +0} \varepsilon \log(e^{\alpha/\varepsilon} + e^{\beta/\varepsilon} + \dots) = \max(\alpha, \beta, \dots).$$

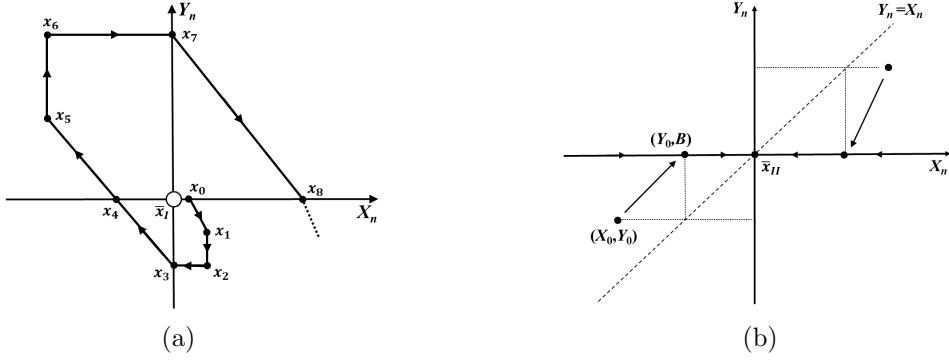


Figure 1: (a) A trajectory in the vicinity of the unstable focus $\bar{x}_I = (B, -B)$, where we set $B = 0$ and $\bar{x}_0 = (1, 0)$. (b) Trajectories obtained from eq.(16).

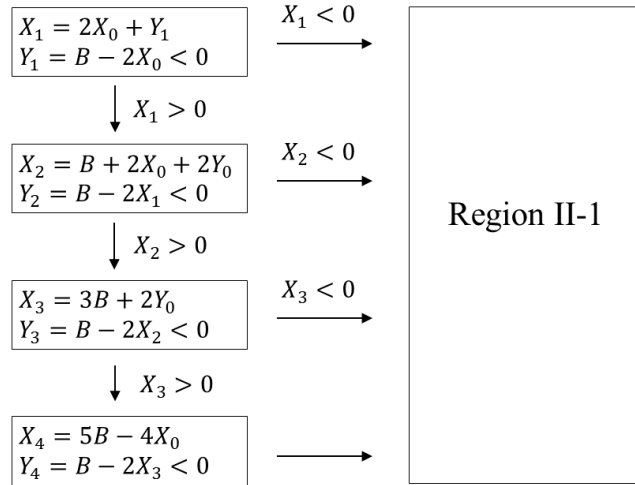


Figure 2: Flowchart for time evolutions of \mathbf{x}_n from the initial state (X_0, Y_0) in region I. (X_0, Y_0) moves into region II-1 within four iteration steps.

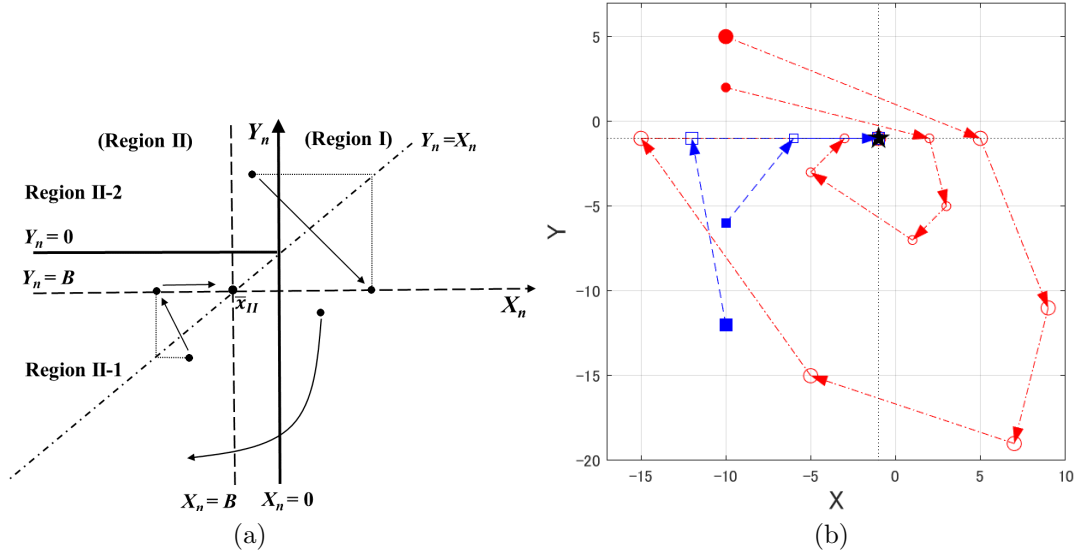


Figure 3: Trajectories obtained from eqs.(13)-(14) with $B \leq 0$. (a) Schematic explanation. (b) Numerical results from four different initial states described by filled circles and squares. Excitability appears when starting from the red filled circles. Here we set $B = -1$. Trajectories proceed in the direction of the arrows and finally reach the stable fixed point $\bar{x}_{II} = (B, B)$ shown by the black star.

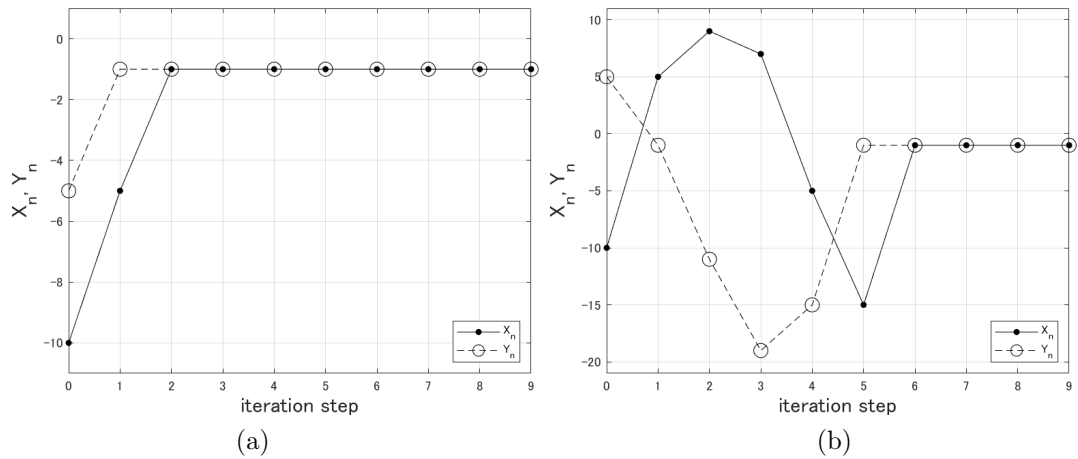


Figure 4: (X_n, Y_n) as a function of n for eqs.(13)-(14) with $B = -1$ from two different initial conditions.

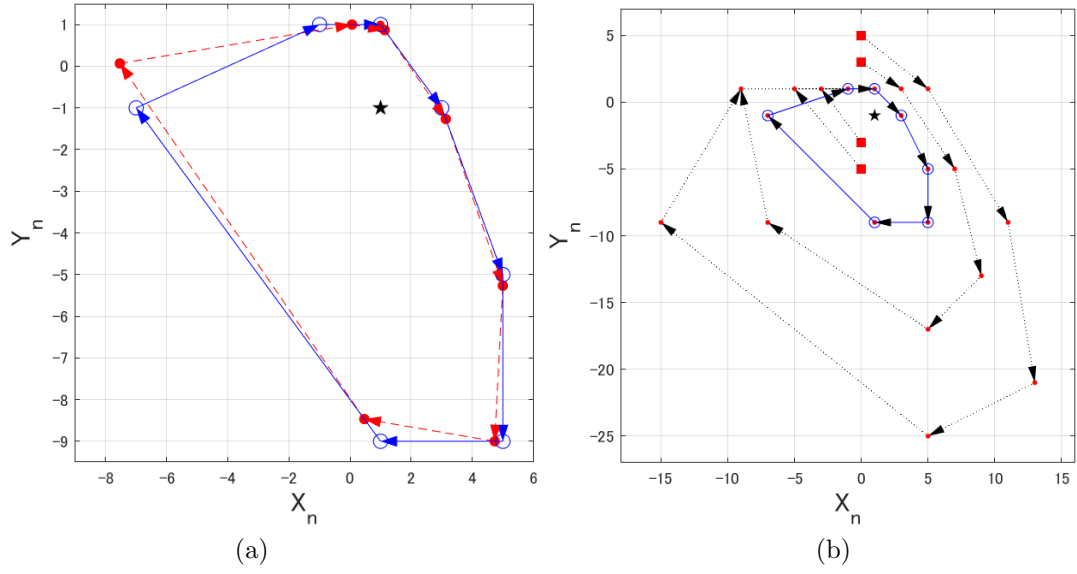


Figure 5: (a) The two limit cycles \mathcal{C} (open circles) and \mathcal{C}_s (filled circles). (b) Examples of trajectories starting from four different filled squares. The trajectories finally converge into \mathcal{C} consisting of the blue open circles. The star in each figure shows $\bar{x}_I = (B, -B)$. Here we set $B = 1$.

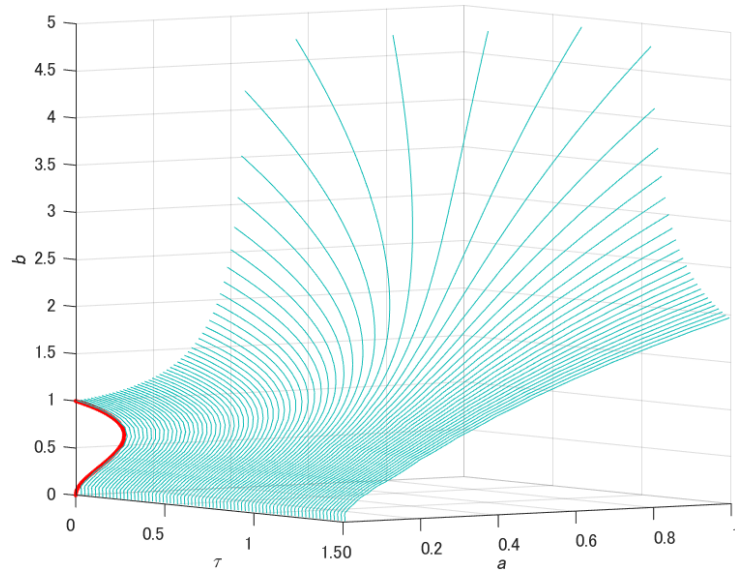


Figure 6: Neimark-Sacker bifurcation surface as a function of a , b , and τ . The red curve shows the Hopf bifurcation curve for the continuous Sel'kov model: $b = b_{\pm}(a)$.

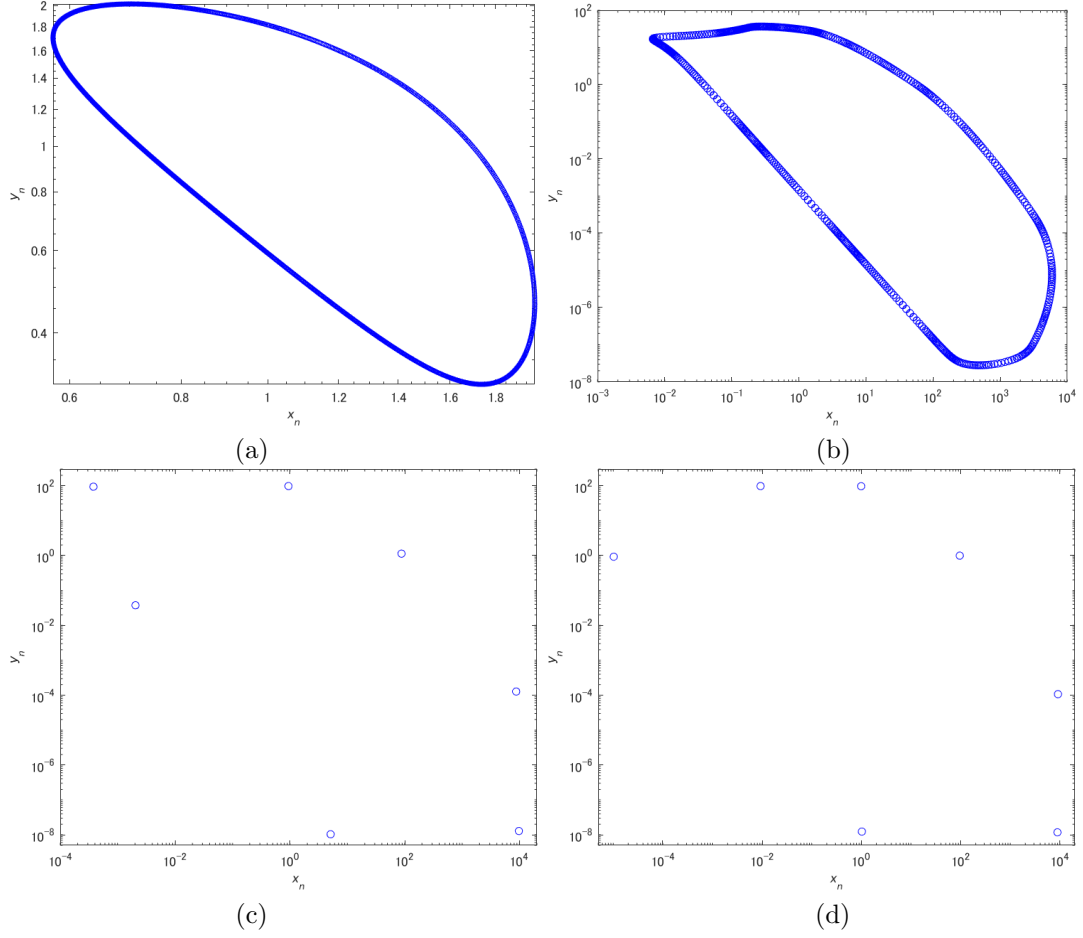


Figure 7: The limit cycles obtained from eqs.(1)-(2) with $a = 0.01$ and $b = 0.98$. The values of τ are (a) 0.1, (b) 25, (c) 2500, and (d) 10^5 . These are plotted with log-log scales.

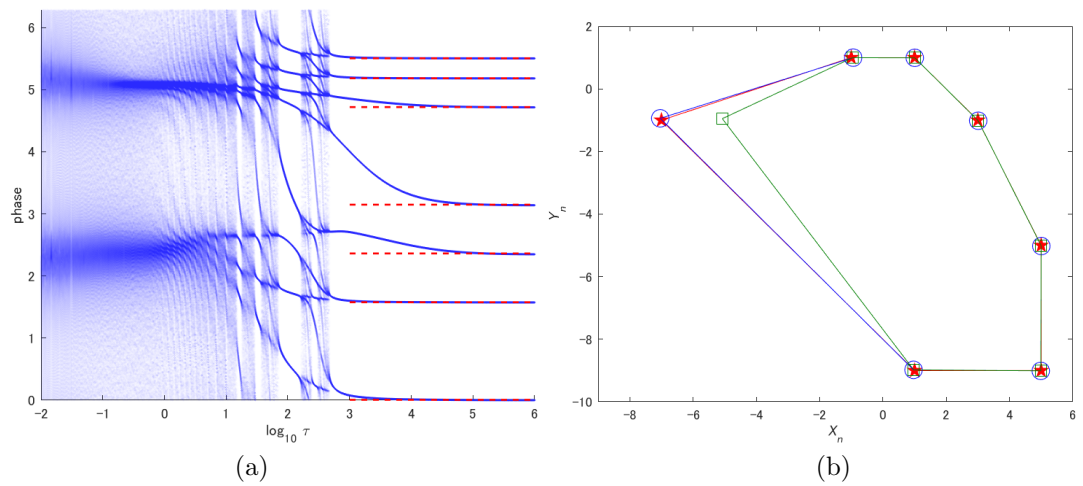


Figure 8: (a) The density of the phase $\{\theta_n(\tau)\}$ in the limit cycles, where $a = 0.01, b = 0.98$. $\theta_n(\tau)$ is defined as eq.(18). The red broken line segments show Θ_n defined as eq.(19). (b) The seven states in the limit cycles. Green open squares show (X_n^*, Y_n^*) from eqs.(1)-(2) for $a = 0.01, b = 0.98$, and $\tau = 10^6$. Blue open circles show (X_n^*, Y_n^*) from eqs.(21)-(22). Red stars show (X_n, Y_n) in \mathcal{C} from eqs.(13)-(14).